water

MDPI

Article

Carbon Dioxide and Methane Emission into the Atmosphere and Its Relationship with Chemogenic Sedimentation in the Hypersaline Lake Baskunchak (Russia)

Dmitry Gar'kusha [1,*], Yury Fedorov [1], Asya Ovsepyan [1,*], Yury Popov [1], Yury Andreev [2], Boris Talpa [1], Natalya Tambieva [2] and Igor' Myakinnikov [3]

[1] Institute of Earth Sciences, Southern Federal University, 40 Zorge Str., 344090 Rostov-on-Don, Russia; fed29@mail.ru (Y.F.); popov@sfedu.ru (Y.P.); talpabv@gmail.com (B.T.)
[2] Hydrochemical Institute of Roshydromet, 198 Stachki Ave., 344090 Rostov-on-Don, Russia; y.a.andreev@gmail.com (Y.A.)
[3] Department of Information Technologies, Faculty of Informatics and Computer Engineering, Don State Technical University, Gagarin Square, 1, 344003 Rostov-on-Don, Russia; igor.myakinnikoff@yandex.ru
* Correspondence: gardim1@yandex.ru (D.G.); ovsepleat@yandex.ru (A.O.)

Abstract: Baskunchak is a large drainless, highly saline lake located in the Caspian lowland. The chemical and gas composition of water (brine) and bottom sediments lying under a 10 cm layer of salt in the lake has been studied; specific fluxes of CH_4 and CO_2 at the water–atmosphere interface have been measured. The lake's sodium chloride brine is characterized by high mineralization (313.5–334.7 g/L) and a slightly acidic–neutral pH (5.75–6.80). Bottom sediments are characterized by a slightly acid–neutral pH (6.27–6.64) and a reducing condition (Eh from −104.7 to +22.0 mV). Specific fluxes of CH_4 into the atmosphere were low (0.11–0.12 mg $CH_4/(m^2\ h)$) due to its low concentrations in the brine of the lake (0.91–2.66 µL/L). The appearance of an excess of HCO_3 during the anaerobic oxidation of CH_4 in the bottom sediments of the lake contributes to the formation of autigenic gypsum and calcite. Specific CO_2 fluxes into the atmosphere ranged from 12.2 to 73.1 mg $CO_2/(m^2\ h)$. The probable source of CO_2 in the brine of the lake and its emission into the atmosphere, in addition to the process of organic matter cycling and uptake by microorganisms, is the chemogenic precipitation of sulfates and calcium carbonates.

Keywords: saline lake; chemogenic GHG emissions; diagenesis; geochemistry of carbon and sulfur; autigenic gypsum and calcite

check for updates

Academic Editor: Guilin Han

Received: 27 December 2024
Revised: 26 February 2025
Accepted: 27 February 2025
Published: 3 March 2025

Citation: Gar'kusha, D.; Fedorov, Y.; Ovsepyan, A.; Popov, Y.; Andreev, Y.; Talpa, B.; Tambieva, N.; Myakinnikov, I. Carbon Dioxide and Methane Emission into the Atmosphere and Its Relationship with Chemogenic Sedimentation in the Hypersaline Lake Baskunchak (Russia). *Water* **2025**, *17*, 738. https://doi.org/10.3390/w17050738

Copyright: © 2025 by the authors. Licensee MDPI, Basel, Switzerland. This article is an open access article distributed under the terms and conditions of the Creative Commons Attribution (CC BY) license (https://creativecommons.org/licenses/by/4.0/).

1. Introduction

Currently, one of the serious environmental problems is global climate change, which causes an increase in tropospheric air temperature, permafrost thawing, a rising sea level, the aridization of continental landscapes, and an increase in the frequency and intensity of hydrometeorological disasters [1]. The climate change observed is largely due to the increase in concentrations of climatically active (greenhouse) gases in the Earth's atmosphere [2,3], among which the largest emission values and contribution to the greenhouse effect are characterized by carbon dioxide (CO_2) and methane (CH_4) at 70% and 23%, respectively [4–7]. According to [8], by 2019, the average atmospheric concentrations of these gases reached 1877 ppb and 410.5 ppm, respectively, representing 260% and 148% of their pre-industrial levels.

As an important source of greenhouse gases, lakes, despite their relatively small areas, can play a significant role in the global balance of greenhouse gas emissions [9].

At present, there is uncertainty in estimating the total CO_2 and CH_4 emissions from the surface of lakes due to both the high spatial and temporal variability of the magnitude and directionality of fluxes of these gases at the water–atmosphere interface [10], as well as insufficient research. Hypersaline lakes (>35 g/L) are particularly poorly studied, the carbon biogeochemistry of which may differ significantly from that of freshwater bodies [11–13]. Hypersaline lakes are usually drainless (terminal). Incoming surface and groundwater runoff, and biogenic and organic substances that formed directly in them, including various salts, mainly remain within their basins [14]. In general, in salt lakes, which occupy a relatively small area compared to freshwater lakes [14], chemical processes such as precipitation, the dissolution of carbonates, and the chemical enhancement of the rate of CO_2 exchange at the air–water interface, due to the hydration of atmospheric CO_2 directly into bicarbonates, are significantly more widespread [13,15]. Under conditions of increasing sulfate in hypersaline lakes, the sulfate reduction process coupled with sulfate-dependent anaerobic methane oxidation becomes more important as the capacity of the anaerobic sulfate–methane transition zone increases [16]. This causes an increase in the "barrier" potential of this zone to contain methane emissions in the system "bottom sediments—water—atmosphere" [17,18].

Baskunchak is a large, drainless, self-sedimenting, hypersaline lake located in the Caspian lowlands, about 270 km north of the Caspian Sea and 53 km east of the Volga River (Figure 1). The area of the lake is about 96 km^2 and the length of the shoreline is 42 km. The lake stretches from northwest to southeast for 16.5 km, with a maximum width of up to 9 km. The surface of the water (brine) in the lake is 21 m below the level of the Caspian Sea. In wet periods of the year (spring and autumn), Lake Baskunchak is a "brine" lake with a maximum level of brine up to 0.7 m [19].

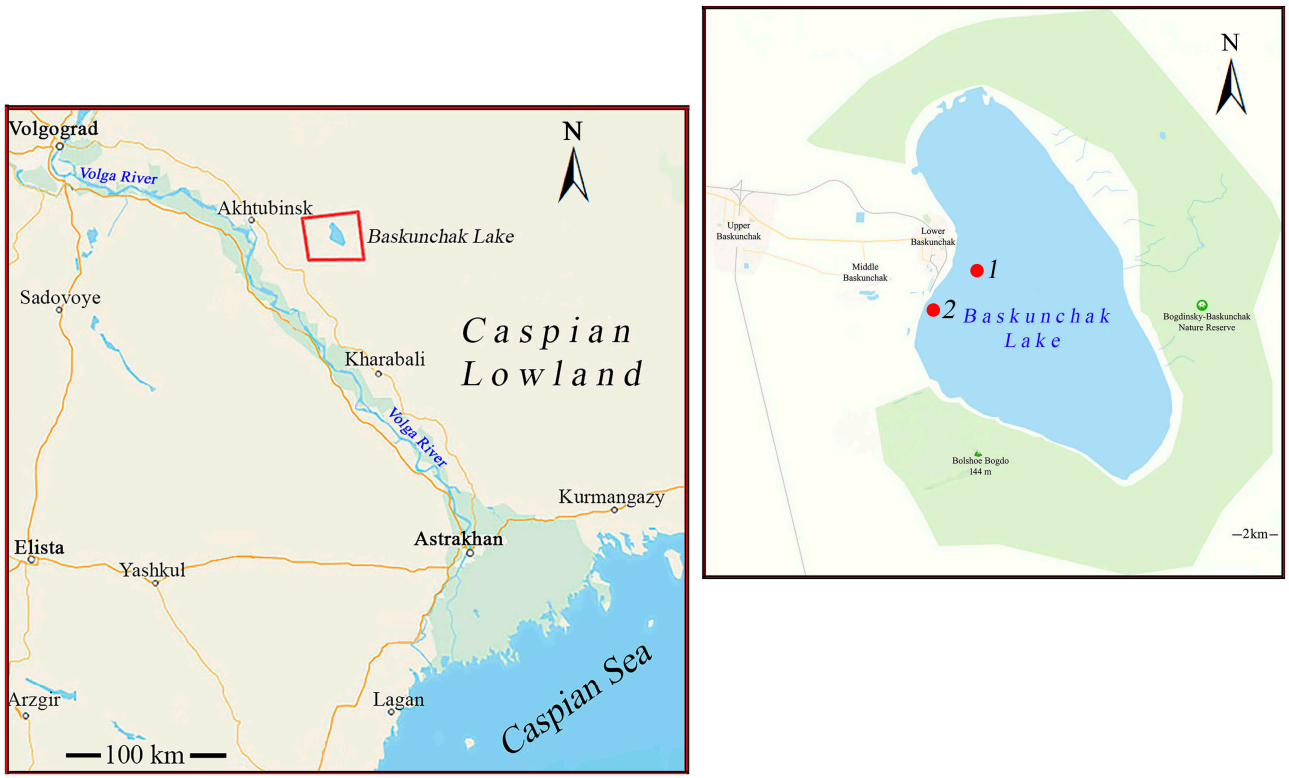

Figure 1. Location of Lake Baskunchak and sampling points in the lake.

The area of Lake Baskunchak is under the predominant influence of continental air masses with low temperatures in winter and dry and hot weather in summer. According to the Verkhniy Baskunchak meteorological station, in the last decade, the coldest months

in the lake area have been January and February (monthly average −5.3 and −3.4 °C, respectively), the hottest have been July and August (monthly average 26.6 and 25.8 °C, respectively). The annual amplitude of air temperature fluctuations reaches 80 °C (from −36 to 44 °C). Within the catchment area of the lake, precipitation averages 265 mm/year. The minimum amount of precipitation is typical for August and November, with the maximum seen in May and July. Summer precipitation, as a rule, falls in the form of heavy showers, which, entering the warmed soil, quickly evaporate and do not play a noticeable role in moisture. According to [20], evaporation in the region is 210–220 mm/year, and the evaporation rate is 820 mm/year.

The lake Baskunchak originated in the western part of the Caspian lowland as a result of salt dome tectonics as a compensatory depression (mulda) located between salt domes and it has a thickness of Quaternary lake sediments over 270 m [20]. These sediments are alternations of terrigenous rocks of marine genesis (sandy and clay) and chemogenic salt rocks (lake salt) formed during the periods of continental breaks [20]. Salt domes of this area have similar structures and are represented by halite strata (according to geophysical data their thickness exceeds 800 m), overlain by gypsum deposits varying in thickness from 10 to 80 m. The depth of the "gypsum cap" varies from 0 to 50 m [20].

The salinity of Lake Baskunchak is more than 300 g/L [19,21–23]. According to the chemical composition, the lake brine belongs to the chloride water class, sodium water group, with some changes in the ionic composition during the year—increases or decreases in SO_4^{2-}, Ca^{2+}, and Mg^{2+} ions [19,21]. The extreme salinity of the lake is related to both the inflow of highly mineralized stream waters into the lake and the hot climate, which causes high rates of evaporation. The high salinity of streams is caused by their predominant feeding by waters of underground springs, which are saturated with salt when circulating in the zone of salt bars, and also enriched with sulfates when ascending to the day surface through strongly karsted gypsum-bearing deposits of Permian age, overlying the salt domes [24,25].

The modern sediments of Lake Baskunchak include the upper salt deposit composed of differently cemented halite crystals (98% of NaC1). It has the form of a lens up to 10–18 m thick, wedging out in the direction of the lake shores [19]. The lens fills the entire area of the lake basin and lies directly on the day surface. The salt deposit is underlain by saline silts, clays, and clayey sands. Further, at depths of several meters, there are salt strata of Permian age with thicknesses ranging from several hundred meters to 6 km. Currently, about 1.5 million tons of salt are mined at Lake Baskunchak per year, for the export of which the Baskunchak railroad was specially built. As a result of extraction, up to 8 m deep cavities filled with brine were formed in the salt deposit.

Sparse data on methane concentration in water and bottom sediments of Lake Baskunchak, as well as its emission into the atmosphere, were published by the authors earlier in [22]. These data are included in the present work for analysis.

This paper analyzes the results of determining the chemical and gas compositions of water (brine) and bottom sediments, as well as taking field measurements of methane (CH_4) and carbon dioxide (CO_2) fluxes, in the hypersaline Lake Baskunchak to identify the features and mechanisms of the formation of concentrations and fluxes of these greenhouse gases into the atmosphere.

2. Materials and Methods

2.1. Sampling and Analysis of Water and Bottom Sediments

The lake Baskunchak was investigated in June and October 2023 and in June 2024. During the observation periods, water (brine) and bottom sediments were sampled in the lake at 1.1 km from its shoreline (point 1), and in situ measurements were made of specific

fluxes of CH_4 and CO_2 into the atmosphere. The bottom at the sampling point is covered with an 8–12 cm layer of dense coarse-grained halite of a light gray color; the thickness of the brine varies from 10 to 25 cm depending on the period of research.

In June 2023, the authors opened a 10–12 cm layer of salt at the observation point with a hammer and chisel, under which an 8 cm long core of bottom sediments was taken using a polypropylene tube. During sampling, the tube was pushed into the sediments with maximum force until it stopped. Concentrations of CH_4, sulfide sulfur ($S_{sulfide}$), C_{org}, moisture, density, Eh and pH values, particle size distribution, and the mineral composition of insoluble residue were determined in the sediments under the salt crust. In water, salinity, pH values, temperature, concentrations of CH_4 and dissolved O_2, major ions, and gross and dissolved Fe and Mn concentrations were determined.

Selection, transportation, sample storage, and the subsequent determination of methane and sulfide sulfur were carried out according to certified methods [26–28]. From the selected core of bottom sediments, 1 mL of sediment is collected using a syringe with a cut-off nozzle, which is added to specially designed vials (43 mL for CH_4 and 12 mL for $S_{sulfide}$) with lids. After this, mandatory conservation is immediately carried out for the subsequent determination of the mass fraction of CH_4 and $S_{sulfide}$. The measurement of CH_4 was performed on the gas chromatograph known as "Chromatek-Crystal 5000.2" with an equilibrium vapor dispenser on the flame ionization detector. The measurement of the mass fraction of $S_{sulfide}$ is based on the conversion of bottom sediments sulfides into hydrogen sulfide by the action of hydrochloric acid and the subsequent blowing of hydrogen sulfide with nitrogen of special purity into a sodium hydroxide solution and its determination by a photometric method with N,N-dimethyl-p-phenylenediamine [28]. In this case, the total content of $S_{sulfide}$ includes both the free hydrogen sulfide dissolved in the sludge water (the sum of undissociated molecules H_2S, hydrosulfide ions HS^-, and sulfide ions S^{2-} in strongly alkaline waters) and sulfides of alkali metals, as well as sulfides contained in the solid fraction, which are sulfides of iron and heavy metals, insoluble in water, but soluble in acid. Simultaneously with sampling, a sample of bottom sediments was collected into pre-weighed and numbered bottles to determine the mass fraction of dry sediment (d.s.) and its moisture content. The moisture content of bottom sediments was determined using a moisture analyzer (weight moisture meter) model ML-50 (A&D Co., Ltd., Japan, Tokyo), and density was assessed using laboratory-scale high-accuracy class model VLT-150-P (ZAO "Sartogosm", Saint Petersburg, Russia).

Eh and pH values were measured using the electrodes of a portable pH meter—"Ecotest 2000"—immediately after sampling. The determination of C_{org} content in sediments was performed according to the Tyurin method modified by CINAO [29], with the preliminary removal of chloride ions from sediments.

The content of major ions in water was determined in laboratory conditions according to standard methods [30]. Bicarbonate (HCO_3^-) was calculated after alkalinity measurement by potentiometric titration to a preselected pH (similar to EPA Standard Method section 2320B.1b). Chloride (Cl^-) was measured by the argentometric method with potassium chromate as an indicator (similar to EPA Standard Method 4500-Cl^- B). Sulphate (SO_4^{2-}) was measured by a titration method with barium chloride using orthanyl K as an indicator (similar to Environment Canada 1988, NAQ 16303). Hardness was measured by the EDTA titration method with Eriochrome Black T at pH of 10 (similar to EPA Standard Method 2340 C). Calcium (Ca^{2+}) was measured by ab EDTA titration method with a Murexide at a pH of 12 (similar to EPA Standard Method 3500-Ca B). Magnesium (Mg^{2+}) was calculated as the difference between hardness and calcium titration (similar to EPA Standard Method 3500-Mg B). The sum of sodium and potassium ($Na^+ + K^+$) was estimated by adding negatively charged ions and then subtracting the sum of positively charged ions.

Mineralization was calculated by summarizing positively and negatively charged ions in a sample of water. Concentrations of dissolved oxygen in water and its temperature were measured directly at the water body using a portable oxygen meter known as Mark 303 M.

The measurement of Fe and Mn in unfiltered and filtered samples was performed on atomic absorption spectrometers Shimadzu AA-7000 (Shimadzu Corporation, Japan, Kyoto) (June 2023) [31] and "KVANT—2AT" (June 2024) [32], which allowed the quantitative assessment of dissolved forms of metals and their gross content. Water samples were filtered through pre-cleaned and suspended membrane filter "Vladipor" type MFAS-VA, with a pore size of 0.45 μm, not later than 1 h after sampling. For the subsequent determination of Fe and Mn concentrations in them, filtered and unfiltered water samples of 100 mL each were preserved by adding nitric acid solution 1:1 at a pH $\leq$ 2 in accordance with the method [31]. Before analysis, unfiltered samples were subjected to thermal treatment with the addition of nitric acid and hydrogen peroxide.

2.2. Granulometric and Mineral Composition of Bottom Sediments Study

The separation of granulometric fractions of bottom sediments was performed according to the method [33] in several stages. At the first stage, the weight (140 g) of the quart sample of bottom sediments, brought to an air-dried state, was divided into fractions using a column of sieves with a mesh size of 2, 1, 0.5, 0.25, 0.1, and 0.05 mm, after which the fractions were weighed to the accuracy of hundredths of grams and percent, respectively. At the second stage, the separated fractions were again passed through a column of the same sieves, accompanied by thorough washing with water at a temperature of 18–20 °C [33]. As a result, the minerals with good solubility in water were dissolved, and poorly or insoluble minerals were cleaned from dusty particles. The fraction greater than 2 mm was briefly washed with water to purify it from finer particles, but also to prevent the strong dissolution of minerals for subsequent identification. The separated and air-dried insoluble residue of each fraction was weighed, after which the total mineral composition was studied using X-ray phase analysis combined with optical and scanning electron microscopy.

X-ray phase analysis was performed using a general-purpose X-ray diffractometer DRON-7 under copper anode radiation (CuKα1 1.5406 Å). Pre-dried samples were abraded in a ring mill (ROCKLABS Standard Ring Mill) for 2 min at 700 rpm. Scanning electron microscopy was performed using a TESCAN VEGA II LMU electron microscope integrated with an INCA ENERGY 450/XT energy-dispersive microanalysis system. The prepared samples (polished briquette beads and bottom sediment samples poured in a thin layer on double-sided electrically conductive carbon tape) were sputtered with carbon (15 nm) and studied at an accelerating voltage of 20 kV. The complex of studies was carried out on the basis of the Center for Collective Use of Scientific Equipment "Center for Research of Mineral Raw Materials and Environmental Conditions" of the Southern Federal University, Rostov-on-Don.

2.3. Measurements of Methane and Carbon Dioxide Specific Fluxes

The specific flux of methane and carbon dioxide from the surface of the Lake Baskunchak brine was determined by the chamber method using accumulation chambers, specifically traps [34,35] (Figure 2). The traps are polycarbonate containers of cylindrical shape with an open base on floats made of foam for stability on the water.

The specific fluxes of CH_4 and CO_2 were calculated from the rate of change of their concentrations in the air phase of the chambers, taking into account "idle" samples taken immediately after the traps were set (0 min exposure) according to [34,36,37].

Figure 2. Lake Baskunchak, point 1, June 2024. In the background is Mount Bolshoe Bogdo. The photo show a graduate student at the Southern Federal University (Rostov-on-Don, Russia), E.A. Kovalev, during the installation of the storage chamber.

In 2023, two traps were used for CH_4-specific flux measurements: one was used in June with an air volume of 1430 cm^3 and a base area of 196 cm^2 and one was used in October with a volume of 3600 cm^3 and a base area of 539 cm^2. The tops of both traps at CH_4 have a sealed plastic lid with diameters of 4 and 6 cm depending on the size of the trap. The lid has a special hole up to 1 cm in diameter, blocked by a 1.5 mm thick rubber gasket, for gas phase extraction by a syringe. After placing the traps on the water surface, the lid is closed. Immediately before (0 min exposure—"blank" sample) and after a certain interval 2.5 mL of the gas mixture sample is taken with a syringe and injected into standard glass vials for vapor-phase analysis with a preservative [27]. The exposure of traps in the accumulation mode was 30 min in June and 25 min in October.

The specific flux (F) of methane (mg $CH_4/(m^2$ h)) was calculated using the formula:

$$F_{CH4} = ((C_x - C_0) \times V/(S \times t)) \times 60 \times 0.0007, \quad (1)$$

where C_x is the concentration of CH_4 in the accumulation chamber after time t, μL/L; C_0 is the concentration of CH_4 in the accumulation chamber immediately after its installation (blank sample), μL/L; V is the volume of the air phase in the trap, L; S is the area of the base (inlet) of the trap, m^2; t is the duration of trap exposure, min; 0.0007 is the coefficient for converting μL to mg; and 60 is the coefficient for conversion into hours, min/h.

A storage chamber with an air phase volume of 1750 cm^3 and a base area of 196 cm^2 was used to measure the specific flux of CO_2 in June 2023. The top of the trap has a special opening with a silicone hose hermetically inserted into it, ending with a three-way valve that is closed for the exposure period. At a certain interval, the silicone hose of the portable infrared gas analyzer PGA-1 is connected to the three-way valve to take the gas mixture from the trap. Before measurement, the gas analyzer is pumped with nitrogen (99.9999%) to set the zero. The PGA-1 gas analyzer is equipped with a calibration chamber, a silicone

hose, and a blower for forced gas phase intake using the built-in microcompressor. The measuring range of the CO_2 volume fraction is from 0 to 2 vol. %; the operating temperature range is from −30 to +35 °C; the time of reading establishment is 30–60 s. The exposure of the trap to CO_2 in the accumulation mode was 30 min.

A storage chamber with an air phase volume of 6000 cm^3 and a base area of 539 cm^2 was used to measure the specific fluxes of CH_4 and CO_2 in June 2024. In the upper part of this trap, there is also a special hole up to 1 cm in diameter, hermetically sealed with rubber, through which a syringe is used to take a sample of the gas mixture for the determination of CH_4 concentrations according to the scheme described above. To measure CO_2 concentrations inside the storage chamber, there is a measuring module consisting of Freenove ESP32 microcontroller (hereinafter referred to as ESP32), Sensirion SCD30 sensor measuring CO_2 concentration, BME280 pressure sensor, and a module for microSD memory card connection. Sensirion SCD30 and BME280 sensors are connected to the microcontroller via the I2C bus memory card module and via SPI bus. Each of the sensors (Sensirion SCD30 and BME280) uses original built-in sensors for temperature and humidity measurement, which allows the independent control of these parameters.

The calculation of the specific flow (F) of carbon dioxide (in mg $CO_2/(m^2\ h)$) is performed using the formula [36]:

$$F_{CO2} = c_2 \times P \times M \times (C_x/T_x - C_0/T_0) \times V/(t \times S), \quad (2)$$

where C_x is the concentration of CO_2 in the accumulation chamber after time t, ppm; C_0 is the concentration of CO_2 in the accumulation chamber immediately after its installation, ppm (blank sample); T_x is the temperature in the accumulation chamber after time t, °Kelvin; and T_0 is the temperature in the accumulation chamber immediately after its installation, °Kelvin. To convert the temperature from [°C] to [°K], it is necessary to add T in °C to 273.15; c_2 is the conversion factor equal to 0.12 mg·mol·K/(kg·J·ppm); P is the pressure in the accumulation chamber, Pa; M is the molar mass of CO_2 (0.048), kg/mol; V is the volume of the air phase in the accumulation chamber, m^3; t is the exposure time of the accumulation chamber, h; and S is the area of the base of the accumulation chamber, m^2.

3. Results and Discussion

3.1. Results of the Study of Water and Bottom Sediments of Lake Baskunchak

The waters of Lake Baskunchak are characterized (Table 1) by high salinity (from 318.1 (in October 2023) to 334.7 g/L (in June 2024), a slightly acidic pH 5.75–5.89, and low methane concentrations 0.91–2.66 µL/L (average 1.5 µL/L). Dissolved oxygen concentrations were 3.16–3.24 mg/L, which, taking into account a significant decrease in gas solubility under conditions of extremely high salinity [38], may indicate both good aeration of the low-water column of the lake's brine and low intensity of organic matter oxidation processes.

In the studied 8 cm horizon of saline dark gray silts, opened under the 10–12 cm layer of salt, the fraction with a size greater than 2 mm (74.25% of the total mass) prevailed (Table 2), a significant mass of which is confined to the surface 0–2 cm layer. Short-term water washing of the material of this fraction reduced its mass by 64%, which was mainly due to the leaching of well-soluble halite, and to a lesser extent due to its purification from finer particles. Individual crystals and aggregates of halite up to 20 mm in size were identified in this fraction after short-term washing. When the material of this fraction was dissolved in water for a longer period, one light-colored, translucent, prismatic crystal (about 2 mm) with well-developed faces remained in the insoluble part. No reaction occurred when 10% hydrochloric acid was added. The mineral was identified as gypsum.

Table 1. Results of studies of Baskunchak Lake brine.

No. of Points	Coordinates, N/E	Date of Sampling	Water Temperature, °C/Mineralization, g/L	pH/O_2, mg/L	Concentration of CH_4 in Water, μL/L	CH_4 Fluxes, mg CH_4/(m^2 h)	CO_2 Fluxes, mg CO_2 /(m^2 h)
1	48°12′47.00″/ 46°51′10.55″	June 2023	21.0/320.2	5.75/-	1.19–2.66 (2) *	0. 12	35.3
		October 2023	8.4/318.1	5.75/3.16	1.07	0.11	-
		June 2024	22.5/334.7	5.89/3.24	0.91	0. 12	12.2–73.1 (14)
2 **	48°11′51.90″/ 46°49′48.66″	May 2019	11.0/313.5	6.80/-	0.47–1.43 (2)	-	-

Note(s): *—the limits of change are indicated, with the number of measurements in parentheses. **—data for point 2 are taken from the work [22].

Table 2. Results of the determination of granulometric composition of bottom sediments by the sieve method with and without water washing, point 1, June 2023.

Indicator	Fraction, mm							Total Weight of Fractions
	More than 2	2–1	1–0.5	0.5–0.25	0.25–0.1	0.1–0.05	Less than 0.05	
Fraction content without washing, %	74.3	12.9	6.1	4.3	2.0	0.3	0.1	100
Fraction content after washing, %	26.9	0.2	0.6	1.7	2.9	1.3	66.4	100

The weight of fractions 2–1, 1–0.5, and 0.5–0.25 mm decreased by 98, 90 and 60%, respectively, after washing with water. There was no reaction when 10% HCl was added. The insoluble residue of these fractions is mainly represented by light-colored transparent and translucent rhomboidal and prismatic crystals of gypsum (Figures 3 and 4) with well-developed facets and pelletized quartz grains. The shape of the gypsum crystals and the absence of traces of mechanical transport on their facet surfaces, as well as the paragenetic association with halite, indicate its authigenic origin [39]. The facet surfaces of gypsum crystals do not have traces of dissolution and recrystallization and do not contain inclusions of other mineral phases, which indicates the absence of late diagenetic transformations. Differences in the morphology of gypsum crystals may be related to the growth rate, or to changes in the chemical composition of mud water [40–42]. The good roundness of quartz grains is a consequence of their transportation from the catchment surface. In addition to light-colored aggregates, brown-black and brown aggregates of aqueous iron oxides in association with halite are very rare in the insoluble residue of these fractions.

The mass of fractions 0.25–0.1 and 0.1–0.05 mm after washing, on the contrary, increased by 1.41 and 4.29 times, respectively. The insoluble residue of the 0.25–0.1 mm fraction as well as larger fractions is mainly represented by light-colored transparent and translucent rhomboidal and prismatic crystals of gypsum and fossilized quartz grains (Figure 5a, sample 152). The insignificant magnetic part of this fraction is represented by black- or brown-colored aggregates of aqueous iron oxides.

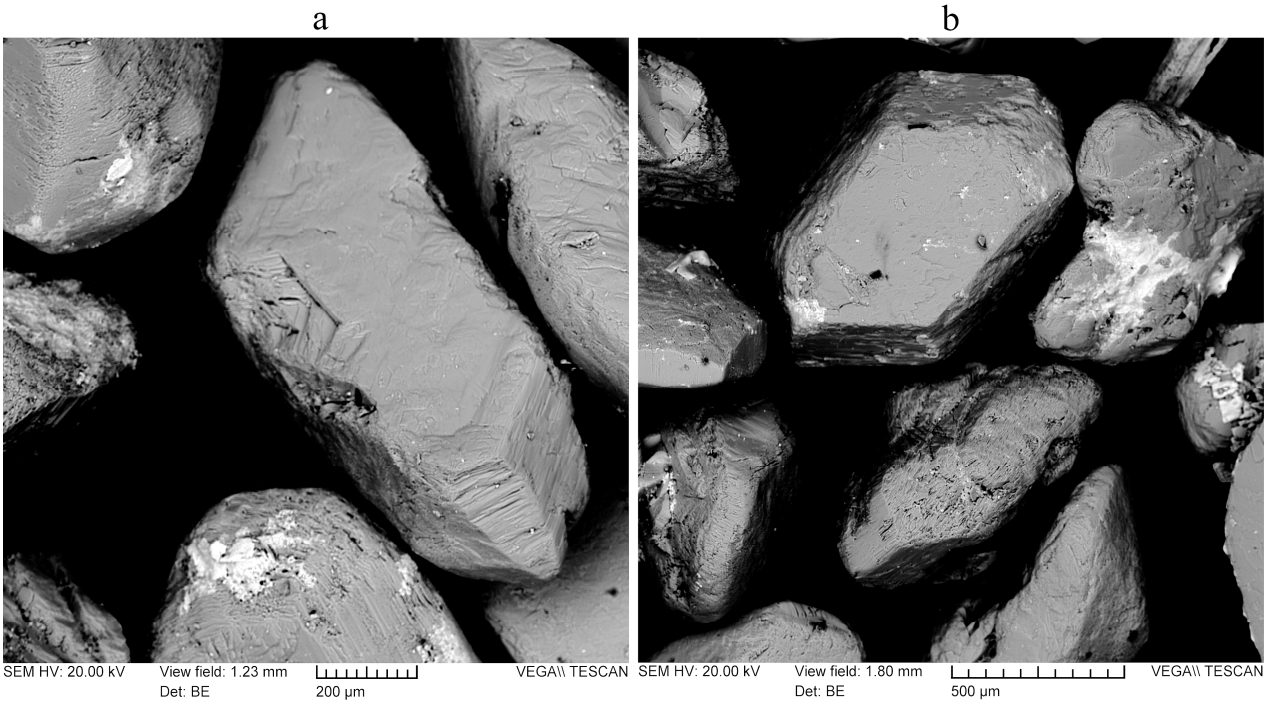

Figure 3. Authigenic gypsum crystals. Backscattered electron images. The light phase on their surface is halite. Scale: (**a**) in 1 cm 200 µm, (**b**) in 1 cm 500 µm.

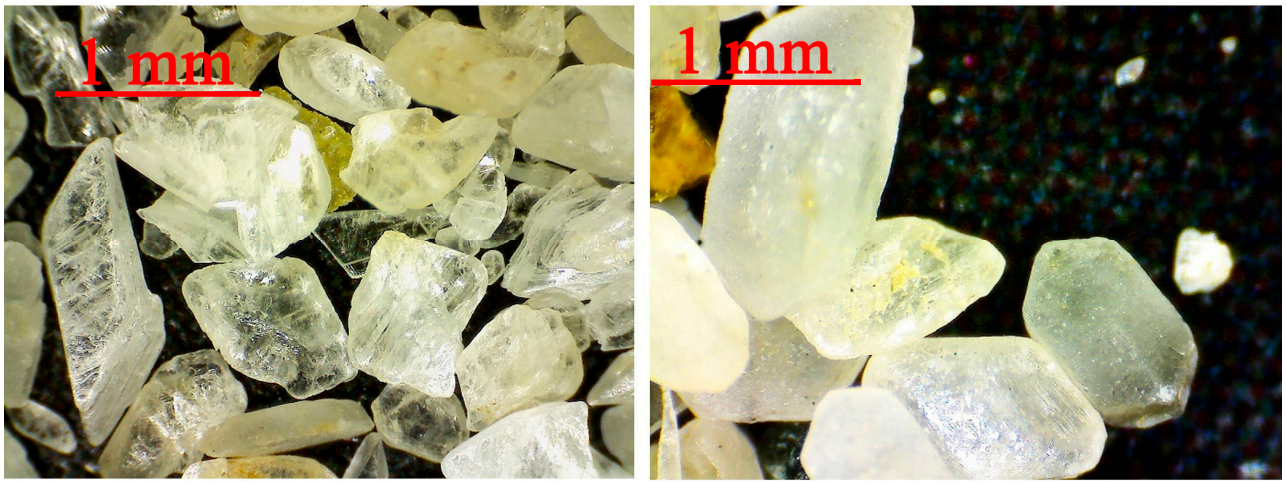

Figure 4. Micrographs of light-colored minerals of the insoluble residue of the 1.0–0.5 mm fraction.

The insoluble residue of the 0.1–0.05 mm fraction is mainly represented by yellowish quartz siltstone. X-ray phase analysis showed the presence of calcite in the insoluble residue of this fraction, in addition to gypsum and quartz (Figure 5b, sample 153).

The mass of the fractions less than 0.05 mm (90.16 g) was calculated by the difference between the mass of all fractions before washing with water (135.72 g) and the mass of fractions greater than 0.05 mm after washing (45.56 g). This mass included both the water-dissolved part of bottom sediments, mainly represented by halite, and particles of clay minerals. The fraction after sieving through a sieve without washing with water was a fine, yellow dust that boiled vigorously after addition of 10% HCl.

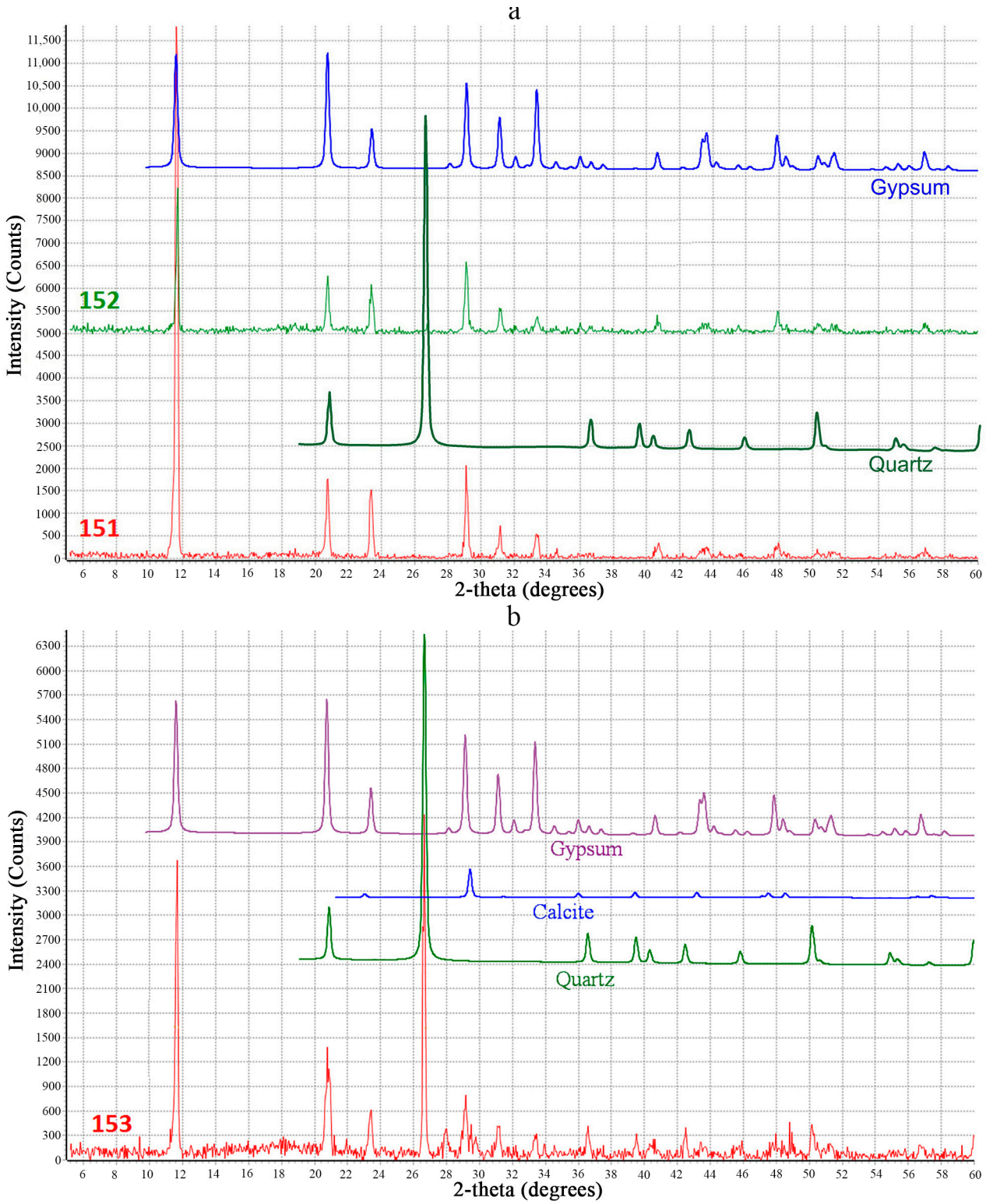

Figure 5. Diffractograms of insoluble residue of self-sedimented salt ((**a**), sample 151) and fractions 0.25–0.1 mm ((**a**), sample 152) and 0.1–0.05 mm ((**b**), sample 153) of bottom sediments of Lake Baskunchak. The diffractograms of the identified mineral phases from the radiographic database PDF-2 are given.

The values of the studied physico-chemical parameters in the bottom sediments of Lake Baskunchak are as follows (Table 3): humidity 9.7–23.6% (average 17.2%); density 1.44–2.78 g/cm^3 (average 1.90 g/cm^3); pH 6.27–6.64 (average 6.42); Eh −104.7 to +22.0 mV (average −60.5 mV); concentrations of C_{org} 1.95–1.97% (average 1.96%); CH_4

0.12–0.28 μg/g d.s. (average 0.18 μg/g); $S_{sulfide}$ 0.036–0.282 mg/g d.s. (average 0.153 mg/g). At the same time, the mass fraction of CH_4 in the studied subsalt sediment layer decreases in the direction from the surface to the lower horizon, and $S_{sulfide}$, on the contrary, increases as Eh decreases.

Table 3. Values of physico-chemical parameters of bottom sediments of Lake Baskunchak at point 1, June 2023.

Horizon, cm	Density, g/mL	Moisture, %	pH	Eh, mV	Corg., mg/g	CH4, μg/g	Ssulfide, mg/g
0–2	1.44	9.7	6.64	+22.0	-	0.28	0.036
2–5	1.47	23.6	6.27	−98.7	1.95	0.15	0.141
5–8	2.78	18.4	6.34	−104.7	1.97	0.12	0.282

The values of the studied hydrochemical parameters of water and bottom sediments agree well with the results of studies conducted by the authors [22] in May 2019 (see Table 1) in Lake Baskunchak at a distance of 0.3 km from the shoreline of the lake (point 2). At this point, the thickness of the brine did not exceed 15 cm, and the bottom was covered with a 1–2 cm crust of hard coarse-grained halite from pure white to light gray. Beneath the salt crust, underlain by a 0.1 cm layer of brown silt, there was black, moist, fine-grained silt without hydrogen sulfide odor, in the surface horizon (0–2 cm) of which the methane concentration was 0.01 μg/g dry sediment. The mineralization of lake water during this period was slightly lower than in the summer–autumn period of 2023 and 2024 and was 313.5 g/L, pH −6.67. The methane concentration in the water varied within the range of 0.47–1.43 μL/L.

In general, the waters of Lake Baskunchak are characterized by the relative stability of the main components of chemical composition (Table 4), with slightly higher mineralization in summer and minimum mineralization in spring, which agrees with the studies [21].

Table 4. Results of Baskunchak lake brine studies.

Observation Point	Date of Sample Collection	Mineralization, g/L	Hardness, g-eq/L	HCO_3^-, g/L	Cl^-, g/L	SO_4^{2-}, g/L
1	June 2023	320.2	1.9	0.06	201.4	1.5
	October 2023	318.1	2.1	0.06	199.5	5.7
	June 2024	334.7	1.7	0.07	209.4	2.9
2	May 2019	313.5	1.5	0.05	195.8	1.2
Observation Point	Date of Sample Collection	Ca^{2+}, g/L	Mg^{2+}, g/L	$Na^+ + K^+$, g/L	Fe Total Dissolved/Gross, mg/L	Mn Total Dissolved/Gross, mg/L
1	June 2023	15.0	13.3	88.8	0.12/0.32	11.7/13.8
	October 2023	8.5	20.2	84.2	-	-
	June 2024	7.0	15.8	99.5	0.15/0.44	10.7/11.4
2	May 2019	6.4	14.7	95.4	-	-

According to O.A. Alekin's classification [43] by chemical composition, the lake waters in all periods belonged to the class of chloride waters, the group of sodium waters, and the third type.

Concentrations of total dissolved Fe in the Baskunchak Lake brine during the summer period of 2023 and 2024 ranged from 0.12 to 0.15 mg/L and amounted to 34.1–37.5% of its gross content. Relatively low concentrations of dissolved iron occur due to the fact that, under conditions of increased dissolved oxygen content in lake brine, oxidized Fe(III) coagulates and falls to the bottom as a colloidal precipitate [44]. In contrast, dissolved manganese concentrations were high, amounting to 10.7–11.7 mg/L (84.8–93.9% of its gross content), indicating the significant aquatic migration of Mn and its concentration in the lake brine under conditions of high salinity, weakly acidic pH, and the oxygen saturation of waters. An important factor of high concentrations of dissolved manganese is the lower iron content in the brine, which limits the flocculation of Fe(III), leading to a significant decrease in the sorption of Mn by colloids–floccules and its deposition to the bottom in the form of a suspension.

3.2. Carbon Dioxide and Methane Fluxes at the Water–Atmosphere Interface and the Mechanisms Responsible for Their Formation in the Hypersaline Lake Baskunchak

Analysis of the change in CO_2 concentrations in the air space of the storage chamber installed on the surface of the lake brine in June 2024 shows that its concentration increased from 384 to 428 ppm, i.e., by 44 ppm, during the 20 min exposure (Figure 6). The specific CO_2 flux calculated from the rate of change in CO_2 concentration in the airspace of the storage chamber was characterized by significant variation, 12.2–73.1 mg $CO_2/(m^2\ h)$. Despite the difference in determination methods, the average value of the specific CO_2 flux in June 2024 (30.7 mg $CO_2/(m^2\ h)$) was close to the CO_2 flux measured in June 2023 (35.3 mg $CO_2/(m^2\ h)$) (see Table 1). On average, the CO_2 flux in Lake Baskunchak is higher than the average CO_2 fluxes (6.1–10.7 mg $CO_2/(m^2\ h)$) from the surface waters of fresh and salt lakes (mineralization up to 200 g/L) located in the Sayan–Altai Mountain region (Tyva Republic, Russia) [45], but lower than the average CO_2 flux (118 mg $CO_2/(m^2\ h)$) from the eutrophic salt lake Daihai (mineralization from 13.4 to 13.9 g/L) located in the Inner Mongolia Autonomous Region (China) [46], as well as from thermokarst lakes (on average 260 mg $CO_2/(m^2\ h)$) located in the permafrost zone in Western Siberia [47]. As in Lake Baskunchak, in all the above lake studies, CO_2 fluxes were measured using floating storage chambers.

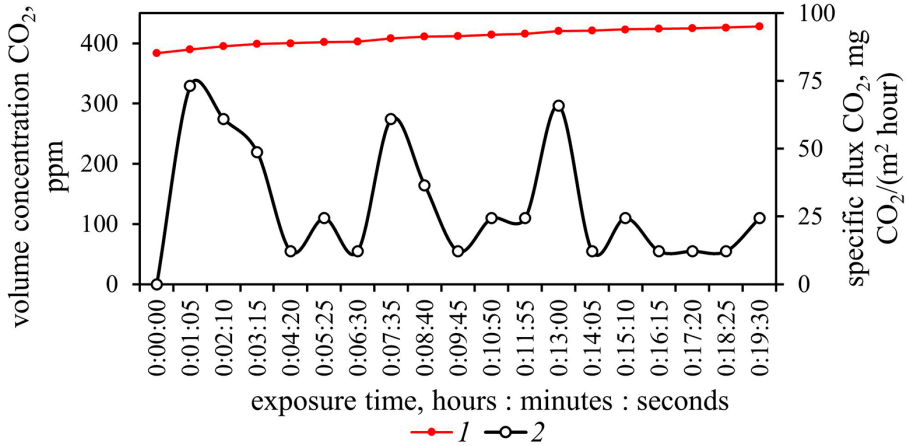

Figure 6. The course of the volume concentration CO_2 in the storage trap chamber (*1*) and its specific flux to the atmosphere (2), June 2024, during the exposure period in Lake Baskunchak.

Specific fluxes of CH_4 to the atmosphere from the lake water surface were stably low during all observation periods and amounted to 0.11–0.12 mg $CH_4/(m^2\ h)$. There are low specific fluxes of CH_4 due to its small concentrations in the lake brine. Thus, comparison with various fresh and mineralized lakes in Russia [11,48–50] shows that

concentrations of CH_4 in the water of Lake Baskunchak are characterized by some of the lowest values. The authors of [22], in addition to the significant decrease in gas solubility under conditions of extreme salinity, attribute this mainly to the insignificant flux of CH_4 from bottom sediments to water, both because of the presence of a layer of salt, preventing its emission, and low concentrations of CH_4 in the subsalt horizons of sediments, from where the gas can diffuse through rapidly tightening cracks in the salt deposit, arising during industrial salt extraction. According to the authors, the main sources responsible for the low concentrations of methane in the brine of Lake Baskunchak may be its input as part of flat runoff and atmospheric precipitation [51], as well as the waters of streams confined to the northwestern, northern, and eastern parts of the lake [18,22,52].

Insignificant concentrations of methane in subsalt anaerobic horizons of bottom sediments may be due to the fact that in saline reservoirs the zone of anaerobic sulfate-dependent methane oxidation is confined to the upper horizons of sediments [18,53]. As a result of anaerobic methane oxidation, along with the reduction in sulfate to hydrogen sulfide, there is the formation of an additional amount of hydrogen carbonate ions and some increase in pore water alkalinity [39,54], which is consistent with our data in terms of pH increase from 5.75–5.89 in lake brine to 6.27–6.64 in sediments:

$$CH_4 + SO_4^{2-} \rightarrow H_2O + HCO_3^- + HS^-. \quad (3)$$

In the conditions of the studied subsalt sediments of Lake Baskunchak, as the present studies have shown, excessive hydrocarbonate ion promotes the new formation of mainly authigenic gypsum and calcite, which is observed both in saline lakes [55,56] and marine basins [39,57–59].

Hydrogen sulfide, which appeared in the zone of anaerobic methane oxidation in the form of hydrosulfide ion (3), quickly binds with reactive iron (mainly Fe^{2+}), forming sulfide (4) and pyrite (5) forms of sulfur in the solid phase of sediments [39,60–63]:

$$Fe^{2+} + HS^- \rightarrow FeS + H^+, \quad (4)$$

$$FeS + S^0 \rightarrow FeS_2. \quad (5)$$

It is believed [60,61] that, in modern sediments, the bulk of sulfide sulfur is in the dispersed state and is represented mainly by hydrotroilite (colloidal acid–soluble iron sulfide), and less frequently by its metastable crystalline modifications—greigite and mackinawite, which later recrystallize into pyrite [64]. Hydrotroilite, being colloidal, unlike pyrite and greigite, is washed out of the insoluble residue during the determination of the granulometric composition of sediments with water washing. Mackinawite, which predominantly occurs as a weakly crystalline sediment, is also likely to be washed out. Apparently, the small amount of iron sulfide minerals in the studied solid phase of sediments of Lake Baskunchak is due to their microscopic size, which causes them to slip through the cells of the used sieves. Iron disulfide microphases can also be present in the aggregates of aqueous iron oxides.

The causes of CO_2 release into the atmosphere from the surface of highly mineralized brine of Lake Baskunchak deserve special discussion. In addition to the process of organic matter degradation by microorganisms [65] capable of living in conditions of extreme salinity, a probable source of CO_2 in the lake brine and its emission into the atmosphere may be chemogenic the precipitation of calcium sulfates and carbonates accompanied by CO_2 release in the course of the following reaction:

$$2Ca^{2+} + 2HCO_3^- + SO_4^{2-} \rightarrow CaSO_4 + CaCO_3 + H_2O + CO_2\uparrow. \quad (6)$$

CO_2 release can also occur during the oxidation of CH_4 by methanotrophic bacteria [11], in which two oxygen molecules are absorbed, and one CO_2 molecule is released:

$$CH_4 + 2O_2 = CO_2 + 2H_2O. \quad (7)$$

However, due to low concentrations of methane in the brine and subsalt horizons of sediments, as well as isolation of the latter by the salt cover, the role of this process as a source of CO_2 in Lake Baskunchak is insignificant.

In the future, the released CO_2 can be involved in a new carbonate cycle or assimilated by photosynthetics. In ordinary marine water bodies, the scale of purely chemical carbonate precipitation is limited, which is attributed [66] to the activity of bacteria, algae, and other more highly organized organisms that, as a result of photosynthesis, assimilate CO_2 dissolved in water, thereby locally lowering its partial pressure and increasing pH:

$$Ca^{2+} + HCO_3^- \rightarrow CaCO_3 + H^+. \quad (8)$$

In this case, a nucleation center (crystalline germ) of carbonates appears on the cell surface of marine organisms and organisms, controlling growth to grow a variety of shells, which, when the organisms die off, accumulate to form organogenic carbonate sediments.

However, under conditions of extreme salinity (>300 g/L), photosynthetic activity and organic matter production in the brine of Lake Baskunchak are suppressed [65], and only bacteria capable of living in salt basins have been identified in it [19]. Even extremophiles living in many salt lakes, such as the unicellular green algae *Dunaliella* (*Dunaliela* spp.) and the gill-feeding crayfish *Artemia salina* (*Artemia salina*), do not survive in such conditions. At the same time, during the study periods, the authors often observe the presence of the latter in less saline waters of streams (up to 180 g/L) flowing into the lake.

Based on the peculiarities of gypsum solubility (increases with temperature increase from 0 to 38 °C, then sharply decreases), seasonal temperature dynamics only affect its sedimentation rates and CO_2 emission intensity, without changing the flow direction at the "brine—atmosphere" boundary. Whereas calcite, possessing retrograde solubility [67], should be most actively precipitated during daytime forty-degree heat, characteristic of the territory under consideration from June to August. During the cold period, on the contrary, its dissolution with CO_2 uptake is possible. The intensity and direction of these processes can probably determine the seasonal dynamics of CO_2 fluxes from the surface of the highly mineralized Lake Baskunchak into the atmosphere.

In general, due to low concentrations of hydrocarbonate ions, the significance of these processes in the lake is small, and the main process is halite deposition, during which CO_2 is not released. According to some scientists [68], in the past, the dominant role in the accumulation of CO_2 in paleoatmospheres could be related to the mass co-precipitation of gypsums in salt basins.

The presence of an insoluble residue admixture in the self-sedimented salt (halite) deposited at the bottom of the lake can testify to the processes of gypsum deposition in Lake Baskunchak. Thus, according to our studies, 1 kg of self-sedimentary salt of the lake at the observation point without clay minerals contained 4.2 g of light-colored insoluble residue that did not react with acid. Electron microscope examination showed the presence of pelletized quartz grains in this residue, as well as prismatic and rhombic crystals of authigenic gypsum. X-ray phase analysis confirmed their presence (see Figure 5a, sample 151). A possible reason for the absence of carbonate minerals, along with the high acidity of the brine, which limits their formation, may be the complete dissolution of newly formed carbonates under conditions of low temperatures in winter [69–71].

The interpretation of *Google Earth* space images showed that the area of brine covering the salt surface of Lake Baskunchak, considering salt mining outcrops, was about 20 km^2

in June 2024. If we take the values of specific fluxes of CH_4 (0.11–0.12 mg $CH_4/(m^2$ h)) and CO_2 (12.2–73.1 mg $CO_2/(m^2$ h) obtained during this period, on average 30.7 mg $CO_2/(m^2$ h)) to the atmosphere from the water surface of Lake Baskunchak, calculated based on the results of the present studies and converted into the entire area of the lake covered with brine (20 km^2), then the emission of these greenhouse gases will be 2.2–2.4 kg CH_4/h (52.8–57.6 kg CH_4/day) and 244–1462 kg CO_2/h (5.9–35.1 t CO_2/day, average 14.7 t CO_2/day).

4. Conclusions

According to the chemical measurements, the Baskunchak lake waters in all periods belonged to the chloride class and the sodium group. At the same time, their mineralization varied in a small range from 313.5 to 334.7 g/L, with slightly higher values in summer and minimum values in spring. The pH of water in the summer–autumn period was slightly acidic (5.75–5.89), while it was neutral in the spring period (6.80).

Specific fluxes of CH_4 into the atmosphere from the lake water surface were characterized by low values—(0.11–0.12 mg $CH_4/(m^2$ h)), which is due to low concentrations of methane in the lake water (0.91–2.66 μL/L. The authors mainly attribute the latter to the insignificant flux of CH_4 from bottom sediments to water, both due to the presence of a salt layer preventing its emission and low concentrations of CH_4 (0.12–0.28 μg/g dry sediment) in the upper pre-salt horizons of sediments, to which the zone of anaerobic sulfate-dependent methane oxidation is confined. Appearance of excess hydrocarbonate ion during anaerobic methane oxidation in the conditions of subsalt sediments of Lake Baskunchak promotes new formation, mainly of authigenic gypsum and calcite.

The specific flux of CO_2 from the surface of the lake water varied between 12.2 and 73.1 mg $CO_2/(m^2$ h). A possible source of CO_2 in the lake water and its emission into the atmosphere, in addition to the process of organic matter degradation by microorganisms capable of living in conditions of extreme salinity, is the chemogenic deposition of calcium sulfates and carbonates. The presence of its authigenic crystals in the insoluble residue of self-sedimented halite deposited in Lake Baskunchak testifies about the processes of gypsum deposition in the lake; it is an object of industrial mining.

Using Lake Baskunchak as an example, it is shown that salt lakes can be emitters of this greenhouse gas due to the lack of CO_2 consumption by photosynthetics. In the light of observed climate change, the salinization of water bodies and salinization of soils in arid landscapes may become an additional source of CO_2 in the atmosphere. At the same time, CH_4 emission is likely to decrease due to the activation of sulfate reduction processes associated with the sulfate-dependent anaerobic oxidation of methane at greater depths of bottom sediments. For more data, please check the Supplementary Materials.

Supplementary Materials: The following supporting information can be downloaded at: https://www.mdpi.com/article/10.3390/w17050738/s1, Figure S1: Lake Baskunchak, 500 m from point 1, June 2024. In the background is the highest elevation of the Caspian lowland, Mount Bolshoe Bogdo (about 152 m above sea level). In the photo are Associate Professor of the Southern Federal University (Rostov-on-Don, Russia) Garkusha D.N. (left) and graduate student Kovalev E.A. (right). Figure S2: A floating storage chamber-trap used to determine specific fluxes of CO_2 and CH_4 at the water-atmosphere interface in June 2024 on Lake Baskunchak. Figure S3: Large (100 cm) and small (50 cm) hand tubes for collecting sediment cores. Large bottles (43 mL) are used to preserve water and sediment samples for subsequent gas chromatographic determination of methane content. Small bottles (12 mL) are used to collect and preserve samples for sulphide sulphur content.

Author Contributions: Conceptualization D.G. and Y.F.; methodology D.G. and B.T.; software I.M.; validation Y.A. and N.T.; formal analysis Y.P.; investigation D.G. and A.O.; writing—original draft

preparation D.G. and Y.F.; writing—review and editing D.G. and A.O.; visualization Y.P.; supervision D.G. All authors have read and agreed to the published version of the manuscript.

Funding: This research was funded by the Russian Science Foundation, grant number 24-17-00038, https://rscf.ru/project/24-17-00038 at the Southern Federal University. The founder is the President of Russia.

Data Availability Statement: The data presented in this study are available on request from the corresponding author due to privacy.

Conflicts of Interest: The authors declare no conflicts of interest. The funders had no role in the design of the study; in the collection, analyses, or interpretation of data; in the writing of the manuscript; or in the decision to publish the results.

References

1. Pachauri, R.K.; Allen, M.R.; Barros, V.R.; Broome, J.; Cramer, W.; Christ, R.; Church, J.A.; Clarke, L.; Dahe, Q.; Dasgupta, P.; et al. *Climate Change 2014: Synthesis Report. Contribution of Working Groups I, II and III to the Fifth Assessment Report of the Intergovernmental Panel on Climate Change*; IPCC: Geneva, Switzerland, 2014; p. 151. Available online: https://research-repository.uwa.edu.au/en/publications/climate-change-2014-synthesis-report-contribution-of-working-grou (accessed on 26 December 2024).
2. WMO. WMO Greenhouse Gas Bulletin (GHG Bulletin)-No. 14: The State of Greenhouse Gases in the Atmosphere Based on Global Observations Through. 2019. Available online: https://library.wmo.int/index.php?lvl=notice_display&id=21620 (accessed on 1 January 2021).
3. Luo, Y.; Zhao, J. Attentional and perceptual biases of climate change. *Curr. Opin. Behav. Sci.* **2021**, *42*, 22–26. [CrossRef]
4. Raymond, P.A.; Hartmann, J.; Lauerwald, R.; Sobek, S.; McDonald, C.; Hoover, M.; Butman, D.; Striegl, R.; Mayorga, E.; Humborg, C.; et al. Global carbon dioxide emissions from inland waters. *Nature* **2013**, *503*, 355–359. [CrossRef] [PubMed]
5. DelSontro, T.; Beaulieu, J.J.; Downing, J.A. Greenhouse gas emissions from lakes and impoundments: Upscaling in the face of global change. *Limnol. Oceanogr. Lett.* **2018**, *3*, 64–75. [CrossRef]
6. Rosentreter, J.A.; Borges, A.V.; Deemer, B.R.; Holgerson, M.A.; Liu, S.; Song, C.; Melack, J.; Raymond, P.A.; Duarte, C.M.; Allen, G.H.; et al. Half of global methane emissions come from highly variable aquatic ecosystem sources. *Nat. Geosci.* **2021**, *14*, 225–230. [CrossRef]
7. Yin, X.; Jiang, C.; Xu, S.; Yu, X.; Yin, X.; Wang, J.; Maihaiti, M.; Wang, C.; Zheng, X.; Zhuang, X. Greenhouse Gases Emissions of Constructed Wetlands: Mechanisms and Affecting Factors. *Water* **2023**, *15*, 2871. [CrossRef]
8. Asaad, S.M.; Inayat, A.; Rocha-Meneses, L.; Jamil, F.; Ghenai, C.; Shanableh, A. Prospective of Response Surface Methodology as an Optimization Tool for Biomass Gasification Process. *Energies* **2023**, *16*, 40. [CrossRef]
9. Xue, J.; Chen, X.; Wang, X.; Sun, X. Fine-Scale Assessment of Greenhouse Gases Fluxes from a Boreal Peatland Pond. *Water* **2023**, *15*, 307. [CrossRef]
10. Sepulveda-Jauregui, A.; Walter Anthony, K.M.; Martinez-Cruz, K.; Greene, S.; Thalasso, F. Methane and carbon dioxide emissions from 40 lakes along a north–south latitudinal transect in Alaska. *Biogeosciences* **2015**, *12*, 3197–3223. [CrossRef]
11. Fedorov, Y.A.; Tambieva, N.S.; Gar'kusha, D.N.; Khoroshevskaya, V.O. *Methane in Aquatic Ecosystems*; Rostizdat CJSC: Rostov-on-Don, Russia; Moscow, Russia, 2005; 330p. (In Russian)
12. Deocampo, D.M.; Jones, B.F. 7.13—Geochemistry of Saline Lakes. In *Treatise on Geochemistry*, 2nd ed.; Holland, H.D., Turekian, K.K., Eds.; Elsevier: Amsterdam, The Netherlands, 2014; Volume 7, pp. 437–469. [CrossRef]
13. Duarte, C.M.; Prairie, Y.T.; Montes, C.; Cole, J.J.; Striegl, R.; Melack, J.; Downing, J.A. CO_2 emissions from saline lakes: A global estimate of a surprisingly large flux. *J. Geophys. Res. Biogeosci.* **2008**, *113*, G04041. [CrossRef]
14. Meybeck, M. Global distribution of lakes. In *Physics and Chemistry of Lakes*; Lerman, A., Imboden, D.M., Gat, J.R., Eds.; Springer: Berlin/Heidelberg, Germany, 1995; pp. 1–35.
15. Wanninkhof, R.; Knox, M. Chemical enhancement of CO_2 exchange in natural waters. *Limnol. Oceanogr.* **1996**, *41*, 689–697. [CrossRef]
16. Knittel, K.; Wegener, G.; Boetius, A. Anaerobic methane oxidizers. In *Microbial Communities Utilizing Hydrocarbons and Lipids: Members, Metagenomics and Ecophysiology*; McGenity, T.J., Ed.; Springer: Cham, Switzerland, 2018; pp. 1–21. [CrossRef]
17. Wallenius, A.J.; Dalcin Martins, P.; Slomp, C.P.; Jetten, M.S. Anthropogenic and environmental constraints on the microbial methane cycle in coastal sediments. *Front. Microbiol.* **2021**, *12*, 631621. [CrossRef]
18. Gar'kusha, D.N.; Fedorov, Y.A.; Tambieva, N.S. Methane and Sulfide Sulfur in Water and Bottom Sediments of Watercourses of the Steppe Zone of the European Part of Russia. *Geochem. Int.* **2024**, *62*, 878–896. [CrossRef]

19. Amosov, P.N.; Aleksandrova, A.V.; Bukharitsin, P.I.; Golovachev, I.V.; Zemlyanskaya, I.V.; Zmitrovich, I.V.; Kaganov, V.V.; Karpenko, N.T.; Kapralov, S.A.; Kulakov, V.G.; et al. *The State and Long-Term Changes in the Natural Environment on the Territory of the Bogdinsko-Baskunchaksky Nature Reserve*; IPK Tsaritsyn: Volgograd, Russia, 2012; 360p. (In Russian)
20. Kurilenko, V.V.; Zelenkovsky, P.S. The Baskunchak Lake mineral salt deposit: Geology, features of modern salt accumulation, mechanisms of nature and subsoil use. Bulletin of St. Petersburg University. *Earth Sci.* **2008**, *3*, 17–32. (In Russian)
21. Motorin, G.S. *Annual Cycles of the Baskunchak Salt Lake and Its Nutrition Issues. Report of the Bassoli Chemical Laboratory*; Proceedings of the All-Union Scientific Research Institute of the Salt Industry; VNIISol Funds: Artemovsk, Russia, 1952; 105p. (In Russian)
22. Gar'kusha, D.N.; Fedorov YuATrubnik, R.G.; Talpa, B.V.; Kovalev, E.A. Concentration and Emission of Methane and Hydrogen Sulfide in Lake Baskunchak, Ulan-Blag Beam Creek and Degassing Groundwater Sources in Spring. Bulletin of Higher Educational Institutions. North Caucasus Region. *Nat. Sci.* **2023**, *3*, 80–92. (In Russian) [CrossRef]
23. Litovsky, V.V. Graviographic study of salt lakes in the Urals and adjacent areas: II. Northern and Western Kazakhstan, Orenburg region. Geochemical and genetic features. *Geogr. Bull.* **2018**, *3*, 5–16. (In Russian) [CrossRef]
24. Zelenkovsky, P.S.; Kurilenko, V.V. Natural and man-made system of the Baskunchak salt lake and features of its resource exploitation. Bulletin of the St. Petersburg University. *Earth Sci.* **2013**, *4*, 33–52. (In Russian)
25. Kucheruk, T.A.; Amelchenko, V.N. Underground fissure-karst waters of the Kungurian stage. *Geol. Geogr. Glob. Energy* **2008**, *4*, 73–75. (In Russian)
26. *RD 52.24.511-2013*; Mass Fraction of Methane in Bottom Sediments. Measurement Technique by Gas Chromatography Using Headspace Analysis. Hydrochemical Institute: Rostov-on-Don, Russia, 2013; 19p. (In Russian)
27. *RD 52.24.512-2012*; Volume Concentration of Methane in Waters. Measurement Technique by Gas Chromatography Using Headspace Analysis. Hydrochemical Institute: Rostov-on-Don, Russia, 2012; 23p. (In Russian)
28. *RD 52.24.525-2011*; Mass Fraction of Sulfide Sulfur in Bottom Sediments. Measurement Technique by Photometric Method with N,N-dimethyl-p-phenylenediamine. Hydrochemical Institute: Rostov-on-Don, Russia, 2011; 26p. (In Russian)
29. *GOST 26213-2021*; Interstate Standard "Soils. Methods for Determination of Organic Matter". Federal State Budgetary Scientific Institution: Moscow, Russia, 2021; 8p. (In Russian)
30. Rice, E.W.; Baird, R.B.; Eaton, A.D.; Clesceri, L.S. (Eds.) *Standard Methods for the Examination of Water and Wastewater*, 22nd ed.; American Public Health Association: Washington, DC, USA, 2012; 1496p.
31. *RD 52.24.377-2021*; Mass Concentration of Aluminum, Beryllium, Vanadium, Iron, Cadmium, Cobalt, Manganese, Copper, Molybdenum, Nickel, Lead, Silver, Chromium and Zinc in Waters. Methodology for Performing Measurements by The Atomic Absorption Method with Electrothermal Atomization of Samples. Hydrochemical Institute: Rostov-on-Don, Russia, 2021; 38p. (In Russian)
32. *PND F 14.1: 2: 4.139-98*; Quantitative Chemical Analysis of Waters. Methodology for Measuring Mass Concentrations of Cobalt, Nickel, Copper, Zinc, Chromium, Manganese, Iron, Silver, Cadmium and Lead in Samples of Drinking, Natural and Waste Waters by Atomic Absorption Spectrometry. State Committee of the Russian Federation for Environmental Protection: Moscow, Russia, 1998; 24p. (In Russian)
33. *GOST 12536-2014*; Interstate Standard "Soils. Methods of Laboratory Determination of Granulometric (Grain) and Microaggregate Composition". Federal Agency for Technical Regulation and Metrology: Moscow, Russia, 2014; 19p. (In Russian)
34. Bastviken, D.; Cole, J.; Pace, M.; Tranvik, L. Methane emissions from lakes: Dependence of lake characteristics, two regional assessments, and a global estimate. *Glob. Biogeochem. Cycles* **2004**, *18*, 12. [CrossRef]
35. Gar'kusha, D.N.; Fedorov, Y.A.; Tambieva, N.S. Computing the methane cycle elements in the aquatic ecosystems of the Sea of Azov and the World Ocean based on empirical formulae. *Russ. Meteorol. Hydrol.* **2016**, *41*, 410–417. [CrossRef]
36. Glagolev, M.V.; Sabrekov, A.F.; Kazantsev, V.S. *Measurement of Gas Exchange at the Soil/Atmosphere Boundary*; Publishing House of Tomsk State Pedagogical University: Tomsk, Russia, 2010; 96p. (In Russian)
37. Wik, M.; Crill, P.M.; Varner, R.K.; Bastviken, D. Multiyear measurements of ebullitive methane flux from three subarctic lakes. *J. Geophys. Res. Biogeosci.* **2013**, *118*, 1307–1321. [CrossRef]
38. Shadrin, N.V. Hypersaline lakes as the polyextreme habitats for life. In *Introduction to Salt Lake Sciences*; Science Press: Beijing, China, 2018; pp. 180–187.
39. Ruban, A.S.; Rudmin, M.A.; Gershelis, E.V.; Leonov, A.A.; Dudarev, O.V.; Semiletov, I.P.; Mazurov, A.K. Authigenic minerals in bottom sediments of the Laptev Sea seep areas. *Proc. Tomsk. Polytech. Univ. Georesources Eng.* **2020**, *331*, 24–36. (In Russian)
40. Haffert, L.; Haeckel, M.; Liebetrau, V.; Berndt, C.; Hensen, C.; Nuzzo, M.; Reitz, A.; Scholz, F.; Schönfeld, J.; Perez-Garcia, C.; et al. Fluid evolution and authigenic mineral paragenesis related to salt diapirism–The Mercator mud volcano in the Gulf of Cadiz. *Geochim. Cosmochim. Acta* **2013**, *106*, 261–286. [CrossRef]
41. Harouaka, K.; Eisenhauer, A.; Fantle, M.S. Experimental investigation of Ca isotopic fractionation during abiotic gypsum precipitation. *Geochim. Cosmochim. Acta* **2014**, *129*, 157–176. [CrossRef]

42. Vogel, M.B.; Des Marais, D.J.; Parenteau, M.N.; Jahnke, L.L.; Turk, K.A.; Kubo, M.D. Biological influences on modern sulfates: Textures and composition of gypsum deposits from Guerrero Negro, Baja California Sur, Mexico. *Sediment. Geol.* **2010**, *223*, 265–280. [CrossRef]
43. Alekin, O.A. *Fundamentals of Hydrochemistry: A Textbook for Universities*; Gidrometeoizdat: Leningrad, Russia, 1970; 444p. (In Russian)
44. Fedorov Yu, A.; Dotsenko, I.V.; Dmitrik, L.Y. Iron in surface and groundwater of the Azov Sea basin. News of higher educational institutions. North Caucasian region. *Nat. Sci.* **2016**, *3*, 91–99. (In Russian) [CrossRef]
45. Byzaakay, A.A.; Kolesnichenko, L.G.; Kolesnichenko, I.I.; Khovalyg, A.O.; Raudina, T.V.; Prokushkin, A.S.; Lushchaeva, I.V.; Kvasnikova, Z.N.; Vorobyev, S.N.; Pokrovsky, O.S.; et al. Dissolved Carbon Concentrations and Emission Fluxes in Rivers and Lakes of Central Asia (Sayan–Altai Mountain Region, Tyva). *Water* **2023**, *15*, 3411. [CrossRef]
46. Li, X.; Yu, R.; Wang, J.; Sun, H.; Liu, X.; Ren, X.; Zhuang, S.; Guo, Z.; Lu, X. Greenhouse gas emissions from Daihai Lake, China: Should eutrophication and salinity promote carbon emission dynamics? *J. Environ. Sci* **2024**, *135*, 407–423. [CrossRef] [PubMed]
47. Serikova, S.; Pokrovsky, O.S.; Laudon, H.; Krickov, I.V.; Lim, A.G.; Manasypov, R.M.; Karlsson, J. High carbon emissions from thermokarst lakes of Western Siberia. *Nat. Commun.* **2019**, *10*, 1552. [CrossRef]
48. Ivanov, M.V.; Rusanov, I.I.; Pimenov, N.V.; Bairamov, I.T.; Yusupov, S.K.; Savvichev, A.S.; Lein, A.Y.; Sapozhnikov, V.V. Microbial processes of the carbon and sulfur cycle in Lake Mogilnoye. *Microbiology* **2001**, *70*, 675–686. (In Russian) [CrossRef]
49. Fedorov, Y.A.; Tambieva, N.S.; Gar'kusha, D.N. Methane as an indicator of the ecological state of a freshwater reservoir (with a special reference to lakes Valdai and Uzhin). *Russ. Meteorol. Hydrol.* **2004**, *6*, 64–71.
50. Gar'kusha, D.N.; Fedorov, Y.A.; Tambieva, N.S.; Andreev, Y.A.; Adzhiev, R.A. Methane Distribution in Lake Baikal Water. *Water Resour.* **2023**, *50*, 400–414. [CrossRef]
51. Gar'kusha, D.N.; Fedorov Yu, A.; Tambieva, N.S. Global methane sink in atmospheric precipitation and its influence on the formation of methane concentrations in aquatic ecosystems. *Int. Res. J.* **2016**, *9–3*, 16–20. (In Russian)
52. Gar'kusha, D.N.; Fedorov Yu, A.; Kovalev, E.A.; Talpa, B.V.; Andreev Yu, A.; Tambieva, N.S.; Krasnova, E.A. Underground sources of the Peshchernaya ravine of Lake Baskunchak: Hydrochemical features and greenhouse gas emissions. News of higher educational institutions. North Caucasian region. *Nat. Sci.* **2024**, *1*, 63–75. (In Russian)
53. Boetius, A.; Ravenschlag, K.; Schubert, C.J.; Rickert, D.; Widdel, F.; Gieseke, A.; Amann, R.; Jørgensen, B.B.; Witte, U.; Pfannkuche, O. A marine microbial consortium apparently mediating anaerobic oxidation of methane. *Nature* **2000**, *407*, 623–626. [CrossRef]
54. Lin, Z.; Sun, X.; Strauss, H.; Lu, Y.; Gong, J.; Xu, L.; Lu, H.; Teichert, B.M.; Peckmann, J. Multiple sulfur isotope constraints on sulfate-driven anaerobic oxidation of methane: Evidence from authigenic pyrite in seepage areas of the South China Sea. *Geochim. Cosmochim. Acta* **2017**, *211*, 153–173. [CrossRef]
55. Popov Yu, V.; Gulov, O.A.; Vasenko, V.A. New data on the structure and composition of the peloid sequence of the Eastern Basin of Lake Saki (Crimea). Problems of mineralogy, petrography and metallogeny. *Sci. Read. Mem. P. N. Chirvinsky* **2015**, *18*, 211–217. (In Russian)
56. Borzenko, S.V. Geochemistry of Salt Lakes of Eastern Transbaikalia. Ph.D. Thesis, National Research Tomsk Polytechnic University, Tomsk, Russia, 2018; 42p. (In Russian)
57. Berner, R.A. *Early Diagenesis: A Theoretical Approach*; Princeton University Press: Princeton, NJ, USA, 1980; Volume 241.
58. Peckmann, J.; Thiel, V. Carbon cycling at ancient methane–seeps. *Chem. Geol.* **2004**, *205*, 443–467. [CrossRef]
59. Wu, D.; Sun, T.; Xie, R.; Pan, M.; Chen, X.; Ye, Y.; Liu, L.; Wu, N. Characteristics of authigenic minerals around the sulfate-methane transition zone in the methane-rich sediments of the northern South China Sea: Inorganic geochemical evidence. *Int. J. Environ. Res. Public Health* **2019**, *16*, 2299. [CrossRef] [PubMed]
60. Volkov, I.I. *Geochemistry of Sulfur in Ocean Sediments*; Nauka Publ.: Moscow, Russia, 1984; 272p. (In Russian)
61. Rozanov, A.G.; Gurskii, Y.N.; Kokryatskaya, N.M. Composition of interstitial waters and forms of sulfur compounds in bottom sediments in the northeastern Black Sea. *Lithol. Miner. Resour.* **2017**, *52*, 249–262. [CrossRef]
62. Peckmann, J.; Reimer, A.; Luth, U.; Luth, C.; Hansen, B.; Heinicke, C.; Hoefs, J.; Reitner, J. Methane-derived carbonates and authigenic pyrite from the northwestern Black Sea. *Mar. Geol.* **2001**, *177*, 129–150. [CrossRef]
63. Rickard, D.; Luther, G.W. Chemistry of iron sulfides. *Chem. Rev.* **2007**, *107*, 514–562. [CrossRef] [PubMed]
64. Berner, R.A. Sedimentary pyrite formation: An update. *Geochim. Cosmochim. Acta* **1984**, *48*, 605–615. [CrossRef]
65. Shadrin, N.; Anufriieva, E. Ecosystems of hypersaline waters: Structure and trophic relations. *Zhurnal Obs. Biol.* **2018**, *79*, 418–427.
66. Bakhtin, A.I.; Kolchugin, A.N. Geochemical features of carbonate sedimentation. *Uchenye Zap. Kazan. Univ. Seriya Estestv. Nauk.* **2011**, *153*, 174–182.
67. Frumina, N.S.; Kruchkova, E.S.; Mushtakova, S.P. *Analytical Chemistry of Calcium*; Nauka Publ.: Moscow, Russia, 1974; 252p. (In Russian)
68. Bessonov, O.A. *Geochemical History of Carbon in the Biosphere (Emergence, Formation and Evolution of the Sphere of Life)*; MP Kniga: Rostov-on-Don, Russia, 1996. (In Russian)

69. Crémière, A.; Pierre, C.; Blanc-Valleron, M.M.; Zitter, T.; Çağatay, M.N.; Henry, P. Methane-derived authigenic carbonates along the North Anatolian fault system in the Sea of Marmara (Turkey). *Deep Sea Res. Part I Oceanogr. Res. Pap.* **2012**, *66*, 114–130. [CrossRef]
70. Pierre, C. The isotopic record of gypsum diagenesis in diluted solutions: Observations in natural salinas and experiments. *Chem. Geol.* **2018**, *493*, 451–457. [CrossRef]
71. Kravchishina, M.D.; Lein, A.Y.; Reykhard, L.E.; Dara, O.M.; Flint, M.V.; Savvichev, A.S. Authigenic Mg-calcite at a cold methane seep site in the Laptev Sea. *Oceanology* **2017**, *57*, 174–191. [CrossRef]

Disclaimer/Publisher's Note: The statements, opinions and data contained in all publications are solely those of the individual author(s) and contributor(s) and not of MDPI and/or the editor(s). MDPI and/or the editor(s) disclaim responsibility for any injury to people or property resulting from any ideas, methods, instructions or products referred to in the content.